Atmos. Chem. Phys. Discuss., 11, 16185–16206, 2011
www.atmos-chem-phys-discuss.net/11/16185/2011/
doi:10.5194/acpd-11-16185-2011

Atmospheric Chemistry and Physics Discussions

Observation of a mesospheric front in a dual duct over King George Island, Antarctica

J. V. Bageston[1], **C. M. Wrasse**[2], **P. P. Batista**[1], **R. E. Hibbins**[3], **D. C. Fritts**[4], **D. Gobbi**[1], **and V. F. Andrioli**[1]

[1]Instituto Nacional de Pesquisas Espaciais (INPE), São José dos Campos, Brazil
[2]Vale Soluções em Energia (VSE), São José dos Campos, Brazil
[3]British Antarctic Survey (BAS), Cambridge, UK, and Norwegian University of Science and Technology (NTNU), Trondheim, Norway
[4]Colorado Research Associates (CoRA), Boulder, USA

Received: 6 May 2011 – Accepted: 25 May 2011 – Published: 31 May 2011

Correspondence to: J. V. Bageston (bageston@gmail.com)

Published by Copernicus Publications on behalf of the European Geosciences Union.

Abstract

A mesospheric bore was observed with an all-sky airglow imager on the night of 9–10 July 2007 at Ferraz Station (62° S, 58° W), located on King George island on the Antarctic Peninsula. The observed bore propagated from southwest to northeast with a well defined wave front and a series of crests behind the main front. There was no evidence of dissipation during its propagation within the field of view. The wave parameters were obtained via a 2-D Fourier transform of the imager data providing a horizontal wavelength of 33 km, an observed period of 6 min, and a horizontal phase speed of 92 m s^{-1}. Simultaneous mesospheric winds were measured with a medium frequency (MF) radar at Rothera Station (68° S, 68° W) and temperature profiles were obtained from the SABER instrument on the TIMED satellite. These wind and temperature profiles were used to estimate the propagation environment of the bore. A wavelet technique was applied to the wind in the plane of bore propagation at the OH emission height spanning three days centered on the bore event to define the dominant periodicities. Results revealed a dominance of near-inertial periods, and semi-diurnal and terdiurnal tides suggesting that the ducting structure enabling bore propagation occurred on large spatial scales. The observed tidal motions were used to reconstruct the winds employing a least-squares method, which were then compared to the observed ducting environment. Results suggest an important contribution of large-scale winds to the ducting structure, but with buoyancy frequency variations in the vertical also expected to be important. These results allow us to conclude that the bore was supported by a duct including contributions from both winds and temperature (or stability). A co-located airglow temperature imager operated simultaneously with the all-sky imager confirmed that the bore event was the dominant small-scale wave event during the analysis interval.

ACPD

11, 16185–16206, 2011

1 Introduction

Mesospheric bore events have been extensively reported at low and mid latitudes (Taylor et al., 1995; Smith et al., 2003; Medeiros et al., 2005; Fechine et al., 2005). Taylor et al. (1995) described a spectacular bore event observed in four mesospheric nightglow emissions at Hawaii (20.8° N) during the ALOHA-93 campaign. Intensity measurements showed that the front was characterized by a sudden increase in the OH brightness and a concurrent decrease in the OI emission. Smith et al. (2003) reported a large-scale, long-duration mesospheric bore over the Southern US which was visible to the naked eye. Medeiros et al. (2005) and Fechine et al. (2005) have reported a large number of mesospheric bore or "front" events (>60) over northeastern Brazilian (7° S) sector over a period of two years.

In contrast, bores are relatively uncommon events at Antarctic latitudes. Nielsen et al. (2006) observed five potential bores in four winter seasons, with only one clear event. That event was seen in airglow images from Halley Station (75.5° S), Antarctica, with responses in three different airglow layers (OH, Na, and O_2), persisted for ~3 h, and exhibited a number of trailing wave crests behind the main front, with an increase in the number of wave crests estimated at ~6.6 crests/hr. The bore characteristics in this case were determined using a standard 2-D spectral analysis and observed wave parameters in the three airglow layers. Because they did not have information about the temperature structure above Halley Station, they could neither infer the duct structure in which the bore was propagating nor identify the presence of inversion layers. Stockwell et al. (2006) applied a S-Transform analysis to the same event reported by Nielsen et al. (2006) in order to investigate the dynamical properties of the bore. They were able to infer the bore parameters (horizontal wavelength, observed horizontal phase speed, and period) and also described its evolution as it propagated. They observed that the horizontal wavelength and horizontal phase speed decreased, and the bore amplitude increased, as the bore evolved.

ACPD
11, 16185–16206, 2011

In our observations at Ferraz Station during 2007, more than 230 gravity wave events were observed (Bageston et al., 2009). The report of only a single bore event, among a large number of gravity wave events, confirms the low occurrence rate of bores at high southern latitudes compared to lower latitudes (Fechine et al., 2005, 2009). This event was classified as a mesospheric bore according to the main characteristics described by Dewan and Picard (1998). It comprised a mesospheric bore having a sharp "front" that extended across the entire all-sky image, with a series of crests following the front and an observed phase speed of 92 m s^{-1}. These features, especially the high phase speed, are in agreement with the characteristics expected for such events (Dewan and Picard, 1998). Zonal and meridional winds observed with a MF radar at Rothera Station (68° S, 68° W), and temperature profiles obtained by the SABER instrument on the TIMED satellite were used to characterize the propagation environment. The results show that the bore was supported by a ducting structure, which is a primary requirement for such events (Isler et al., 1997; Dewan and Picard, 1998; Laughman et al., 2009, 2011). Our analysis and discussion of the bore characteristics and ducting conditions are discussed in detail below.

2 Observations

2.1 Airglow measurements

A mesospheric gravity waves campaign was carried out at Ferraz Station (62.1° S, 58.4° W), located on the King George Island, Antarctica, from May to October 2007, using an all-sky CCD imager. The imaging system uses a 2-inch wide band near infrared (NIR) optical filter (715–930 nm), with a notch at 865.5 nm to suppress the O_2(0–1) emission to measure OH airglow emissions near the mesopause (~87 km). An exposure time of 20 s was used for each image, yielding a sampling interval of ~38 s since the imager does not have a filter wheel. The original images (with 1024×1024 pixels) were not binned, but cropped to 512×512 pixels, due to limitations of the optical

ACPD
11, 16185–16206, 2011

system (Bageston et al., 2009, 2010). The quality of the airglow data and its usage were limited by weather conditions to clear sky and new moon periods.

Our data analysis used here was a slightly modified version of the method described in the literature (Garcia and Taylor, 1997; Medeiros et al., 2003). Initially, a sequence of images was selected in order to analyze the wave event that was previously identified in an animation that contains all the images collected in one night. The star field was subtracted from each image that was selected for analysis, and flat field corrections were applied to the image series. Each image in the data set was spatially filtered with a second-order high-pass Butterworth filter, with cutoff frequencies at 8 and 14 km for projections onto 512×512 km (resolution of 1 km pixel^{-1}) and 768×768 km (resolution of 1.5 km pixel^{-1}) images, respectively. This filtering process was the modification introduced in the methodology. Finally, the observed images were processed using a 2-D Fast Fourier Transform (FFT) analysis, and a cross spectrum was applied to the sequence of images in order to obtain the horizontal wavelength, observed phase speed, and observed period.

2.2 Mesospheric bore event

The mesospheric bore was observed from ~23:20 to 00:00 LT on the night of 9–10 July 2007 at Ferraz Station at the tip of the Antarctic Peninsula as it progressed from southwest to northeast. Figure 1 presents a sequence of three all-sky images for the event observed in the OH emission. The first image at 23:29 LT (LT = UT-3) shows the first clear view of the bore as it crossed the image field. The arrows just ahead of the bore front indicate its propagation direction, i.e., towards the northeast. We emphasize here the difficulty in identifying the bore event in individual images, due to the presence of a thin fog, identified because most of the stars appear defocused (not due to the focus calibration), and the position of the Milky Way approximately centered in the images. These factors made it much more difficult to identify the bore event that otherwise would have been the case. However, the bore structure and propagation were seen clearly in an animation of the event. Due to the limitation of the imager, which

ACPD
11, 16185–16206, 2011

observed the bore with only one filter (OH emission), we were not able to observe the complementarity effect described by Taylor et al. (1995), i.e., an anti-phase relation in the brightness associated with the bore response seen in different airglow layers. From FFT analysis applied to a set of six images from 23:32 to 23:38 (LT), the following bore parameters were obtained: (a) a horizontal wavelength of 33 km, (b) an observed period of 6 min, and (c) an observed phase speed of 92 m s^{-1}. These parameters are very similar to those reported for the bore observed at Halley Station (Nielsen et al., 2006), especially the horizontal wavelength and period, with 31 km and 6.8 min, respectively, seen in the OH layer. The observed phase speed for the bore reported by Nielsen et al. (2006) had a lower limit of 76 m s^{-1}, at the OH airglow layer and lasted for three hours in the images. The parameters calculated by Nielsen et al. (2006) were obtained during the first hour of the bore observation.

2.3 Mesospheric winds

Winds in the mesosphere and lower thermosphere (MLT, ~80–100 km) are known to have large influences on gravity wave and bore propagation in MLT, depending on their propagation direction. Wind measurements were not available at Ferraz during the bore observation. However, mesospheric wind measurements were available with an MF radar at Rothera Station ~765 km to the south, as employed in the study by Bageston et al. (2010). The Rothera MF radar measures horizontal winds in the MLT through analysis of D-region partial reflection echoes (Jarvis et al., 1999; Hibbins et al., 2007). The radar operates at a frequency of 1.98 MHz with a transmitter power of 25 kW and full-width half-maximum pulse width of 25 µs, which corresponds to a height resolution of ~4 km, with returns oversampled at 2 km intervals (Hibbins et al., 2007). Data used here are restricted to altitudes below 94 km as several authors have observed that MF radars tend to underestimate wind speeds compared to those observed by meteor radars at higher altitudes (e.g. Manson et al., 2004 and Portnyagin et al., 2004).

Rothera winds surely do not describe the small-scale winds over Ferraz, but very similar tidal structures are seen at sites with similar spacing extending across the Drake

ACPD
11, 16185–16206, 2011

Passage (Fritts, 2011), and large-scale inertia-gravity waves (IGWs) having vertical wavelengths of ∼10 km or more imply similar structures somewhat shifted in phase at distances up to ∼1000 km or more away. Assuming (as shown below) that tidal and IGW structures dominate the bore ducting environment, Rothera winds will allow us to estimate roughly the intrinsic parameters for the bore.

Winds along the bore propagation direction obtained with the Rothera MF radar during the bore event are shown in Fig. 2a. This profile was obtained by the hourly wind observed during the time duration of bore event, interpolating to 1-km vertical resolution, and then averaging over 3 km in the vertical in order to remove vertical structure expected to not be coherent over large distances. The dominant structure seen has a vertical wavelength of ∼10 km and a near-inertial period (see data analysis and discussion below), suggesting a dominant large-scale IGW with perhaps tidal contributions. Further analysis and discussion of these data and their implications for the bore environment will be provided below.

2.4 Mesospheric temperatures

During Southern Hemisphere winter, SABER views towards high southern latitudes, so measurements are occasionally available very near Ferraz (Russell et al., 1999; Mertens et al., 2004). For this study, the nearest SABER profile was obtained ∼1300 km north of Ferraz, and about 140 min before the bore was seen. This distance is larger than desired, but it is the only profile sufficiently close to Ferraz to be useful, it is likely much more representative of the thermal structure over Ferraz than a climatology without tides would be, and the extent of the bore noted above is greater than the imager field-of-view, suggesting that the ducting environment has a large horizontal extent. This temperature profile is shown in Fig. 2b. The implications of this temperature profile for ducting and bore propagation will be explored further below.

An imaging spectrometer was collocated with the all-sky imager at Ferraz during the bore observation. However, the field-of-view over which the spectrometer temperatures were averaged was ∼70 km in diameter about the zenith, more than twice the

ACPD
11, 16185–16206, 2011

wavelength of the bore identified in the OH images shown in Fig. 1. Hence, the spectrometer showed no evidence of the 6-min bore period inferred from the airglow imager data, and therefore the spectrometer data were not employed in this analysis.

3 Bore analysis and discussion

To investigate the large-scale MLT propagation environment during the bore observation, we use the Rothera MF radar winds and the SABER temperature profile discussed briefly above to compute the vertical profile of m^2, where $m = 2\pi/\lambda_z$ is the vertical wavenumber and λ_z is the local vertical wavelength for positive m^2. The resulting m^2 profile suggests a duct for gravity waves and bores in a region where $m^2 > 0$ that is between two regions having $m^2 < 0$ (in which the relevant motions are evanescent in the vertical) having sufficient depth to cause effective trapping of the disturbance at the m^2 maximum. This was not done in several previous bore studies, including that by Nielsen et al. (2006) at Antarctic latitudes, because of the absence of temperature and/or wind data. The approximate dispersion relation, including wind curvature effects, but neglecting shear effects, is given by

$$m^2 = \left[\frac{N^2}{(u_0 - c)^2} - \frac{u_0''}{u_0 - c} - k_h^2 \right], \quad (1)$$

where N is the buoyancy frequency, u_0 is the horizontal wind in the direction of bore propagation, u_0'' is the second derivative of the wind with altitude, c is the observed phase speed in the direction of propagation, $k_h = 2\pi/\lambda_h$ is the horizontal wavenumber, and λ_h is the horizontal wavelength in the direction of propagation. This dispersion relation is valid for gravity waves propagating in an environment where the effects of horizontal winds and temperature gradients cannot be neglected (Chimonas and Hines, 1986; Isler et al., 1997; Fritts and Yuan , 1989).

ACPD
11, 16185–16206, 2011

The buoyancy frequency, N, can be estimated using the relation 2:

$$N^2 = \frac{g}{T}\left(\nabla T_z + \frac{g}{C_p}\right), \quad (2)$$

where g is the acceleration due to gravity, T is temperature, $C_p = 1005\ J\,kg^{-1}K^{-1}$ is the specific heat at constant pressure, ∇T_z is the vertical temperature gradient, and $\frac{g}{C_p} \sim 9.5\,K\,km^{-1}$ at MLT altitudes.

The vertical profile of m^2 obtained from Eq. 1 for the horizontal wind and temperature profiles shown in Fig. 2a and b is shown in Fig. 2c. Sensitivity to the details of the SABER temperature profile was evaluated by shifting it vertically by ±3 km, that showed a consistence of the duct structure which was also shifted vertically, above and below of the nominal OH peak, but not changing significantly its shape. This suggested that the ducting environment is much more dependent on the structure of the wind profile than on the temperature profile, with the curvature term being particularly important (see below). It is clear from these profiles that the bore event was supported by a large-scale duct between ~83 and 90 km, within which ($m^2 > 0$), with evanescent regions ($m^2 < 0$) above and below. These profiles also suggest that the duct coincides closely with the altitude of the OH airglow layer (Marsh et al., 2006), though we also note that the true ducting environment over Ferraz may have exhibited a different phase structure of the low-frequency motions than observed over Rothera, potentially resulting in a ducting structure centered at somewhat higher or lower altitudes than shown in Fig. 2c.

The observed phase speed of the bore estimated from the 2-D FFT cross spectrum of the airglow images discussed above was $92\,m\,s^{-1}$. This is $\sim 50\,m\,s^{-1}$ faster than the wind along the bore propagation direction at any altitude, and $\sim 70\,m\,s^{-1}$ faster than the mean wind at the center of the primary ducting region (see Fig. 2a and c), where the maximum values of m^2 are implied by the maximum positive temperature gradients (see Fig. 2b). Indeed, temperature inversions, or thermal ducts, have often been associated with mesospheric bores (Dewan and Picard, 1998, 2001; Smith et

ACPD
11, 16185–16206, 2011

al., 2003; She et al., 2004; Smith et al., 2005; Narayanan et al., 2009; Laughman et al., 2009, 2011). The intrinsic phase speed along the direction of propagation implied by the estimated m^2 profile is from ∼50 to 70 m s^{-1}, depending on whether we take the relevant background wind to be the maximum in the direction of propagation or that centered in the ducting region (with $m^2 > 0$). Assuming the latter is most relevant, we infer a corresponding intrinsic period of ∼8 min. The intrinsic parameters of the bore reported by Nielsen et al. (2006) had an opposite variation, since the wind in that case was opposite to the propagation direction, yielding a higher intrinsic phase speed (104 m s^{-1}) and a lower period (5.9 min), compared to our observed parameters.

In a related study, Fechine et al. (2009) performed a comparative analysis of the terms in the dispersion relation for a similar bore observation. They inferred that it was likely supported by a Doppler duct, with apparent influences by the semidiurnal tide. More recently, Bageston et al. (2010) analyzed a mesospheric wall event over Ferraz and concluded that it was supported by a thermal duct, with the winds having little effect on the duct configuration.

We now examine the influences of the wind field we have assumed to apply in the present case in greater detail. Fig. 3 shows a contour plot for the hourly-averaged wind component along the bore propagation direction observed over 24 h from 12:00 LT on 9 July to 12:00 LT on 10 July 2007. The vertical dashed red line at 23:30 LT on 9 July denotes the time when the bore front was near zenith in the all-sky images. This figure indicates both shorter-period motions (periods of ∼4 to 6 h) and longer-period motions (likely IGW or semidiurnal tide winds), with the former achieving the largest amplitudes prior to observation of the bore event. Of the observed motions, we expect that only the lower-frequency components would have had the potential to also occur over Ferraz without large phase and amplitude variations. This is because large horizontal winds imply relatively large vertical wavelengths and shorter observed periods imply smaller horizontal wavelengths. Assuming that the observed periods are indicative of comparable intrinsic periods, this would result in much less coherence at large horizontal distances. Thus, we focus on the longer-period motions hereafter.

ACPD
11, 16185–16206, 2011

A Morlet wavelet analysis (Torrence and Compo, 1998) was used to identify the dominant low-frequency oscillations centered on the day and time of the bore observation. We used a wind time series at 86 km near the center of the duct extending over ~3 days, from 00:00 LT on 9 July to 18:00 LT on 11 July, for this purpose.

Figure 4a shows the result of the Morlet wavelet spectral analysis of the wind time series presented in Figure 4b (black line). The power spectrum describes periods from 4 and 33 h as functions of time. Solid black lines indicate regions where the confidence level is higher than 90%, while the dashed black lines define the region where the results are confident excluding the border effects. The white vertical dashed line indicates the time when the mesospheric bore was seen in the zenith by the all-sky imager. Clearly seen in Fig. 4a is a maximum in spectral density centered at a period of ~10 h, consistent with dominance of the wind field by some combination of IGWs and semidiurnal and terdiurnal tides at this time. Motivated by this result, a band-pass filter was applied to the original wind time series at 86 km high for periods between 6 and 14 h. The filtered time series is shown as a red line in Fig. 4b, and is seen to be consistent with the periodicities observed in the unfiltered time series in Fig. 4b. These results suggest that if the wind was important in defining the ducting structure, then the low-frequency IGW and tidal contributions would have played key roles. The relative importance of the tidal winds and the thermal structure in defining the ducting environment is discussed further below.

In order to assess the tidal contributions to the m^2 profile and potential influences on bore ducting, we employ the least mean square method, which makes use of the well established classical harmonic fitting. Details of this method and the equation employed for fitting the winds (and consequentely to obtain the tidal amplitudes and phases) are found in the work of Andrioli et al. (2009). Following this methodology we are able to reconstruct the wind profiles by means of the amplitude and phase associated to the tidal modes. In our case, it was identified that only the semi-diurnal and terdiurnal modes were present around the observation time of the mesospheric bore and these periodicities were used to reconstruct the vertical wind profiles near the time

ACPD
11, 16185–16206, 2011

in which the wave was seen in the all-sky images. We did not evaluate the contribution from the low-frequency IGW apart of the tides, since the winds reconstruction using just the tidal oscillations produced a good fit in comparison to the observed wind (see Fig. 5b). The winds reconstruction was performed in two ways, at first the tidal components were included, and later the wind contribution due to the tides was removed in order to observe the relative contribution of the tides in the observed duct. Here, the mean wind field was defined as the wind field smoothed as described above after removal of the tides. The mean wind defined here did not includes the low-frequency motions, since its periods were not included in the harmonic fitting.

The resulting m^2 profiles, wind profiles averaged from 23:00 to 24:00 LT on 9 July, and curvature terms are shown in Fig. 5a, b, and c, respectively. In the plots, black lines denote the profiles employing the full wind field as observed with the MF radar (which include tides, low-frequency IGWs and other low-frequency motions), blue lines denote results using only the mean wind, and red lines denote results using the tidal winds added to the mean wind. The buoyancy frequency squared and the corresponding term in the dispersion relation assuming the full wind field with filtered low-frequency motions are shown with red and black lines, respectively, in Fig. 5d.

Comparing the various profiles in Fig. 5, we see that all exhibit a region of maximum (positive) m^2 at altitudes ~84 to 90 km, despite the varying contributions of wind magnitudes and curvature. This implies a significant role of the large and sustained temperature gradient spanning these altitudes in defining the ducting structure. We also see much smaller differences between the black and red profiles in panels (a), (b), and (c) than between the black and blue profiles. The blue profile of m^2 suggests that there is no evanescent region adjacent to the duct at lower altitudes, and that this structure may not support ducted or bore responses at all. This indicates that the tides and low-frequency motions make a significant contribution to the ducting structure enabling bore propagation, particularly in combination with the enhanced stability (and temperature gradient) at the ducting level. Even if the velocity field over Ferraz is somewhat different in phase (and altitude) than measured over Rothera, we expect

ACPD
11, 16185–16206, 2011

the low-frequency IGW and tidal motions to impose ducting structure similar to that shown in Fig. 5, given the apparent importance of the wind and curvature terms in the dispersion relation, provided that some portion of the implied increase in m^2 due to the wind field coincides with the stability enhancement between ~84 and 90 km. Together, these results imply a duct that depends on both the wind and temperature fields, consistent with expectations of theoretical studies of these dynamics (Fritts and Yuan , 1989; Laughman et al., 2009).

4 Conclusions

We described a bore event observed by an all-sky airglow imager over Ferraz Station on the night of 9–10 July 2007. The ducting environment was assumed to be of large spatial extent, given the extent of the bore itself across the full field of view of the imager. We thus employed winds measured at Rothera Station at the south of Ferraz and a temperature profile measured by SABER on TIMED at north, and somewhat earlier than the bore observation, to evaluate the environmental factors likely to have enabled the bore propagation. Our analysis revealed that tidal motions and low-frequency IGW were likely responsible for the wind structure contributing to the ducting environment, but that a maximum in N^2 due to a large positive temperature gradient (~40 K extending over ~6 km) also contributed to the dual thermal and wind duct supporting bore propagation. In particular, the winds were found to be essential in defining the ducting environment in this case, in contrast to other bore events where the temperature structure alone appeared to be sufficient to enable ducting. Future observations at Ferraz Station will benefit from local wind measurements by a new meteor radar recently installed at that site.

ACPD
11, 16185–16206, 2011

Supplementary material related to this article is available online at: http://www.atmos-chem-phys-discuss.net/11/16185/2011/acpd-11-16185-2011-supplement.zip.

Acknowledgements. J. V. Bageston thanks CNPq for post-doctorate project, process no. 151593/2009-4, and to FAPESP, process no. 2010/06608-2, that partially supported the present study. C. M. Wrasse thanks to CNPq for the Grant 304277/2008-8. The present research combines results of the INCT-APA (CNPq process no. 574018/2008-5, FAPERJ process no. E-26/170.023/2008) in the project "Study of the Mesosphere, Stratosphere and Troposphere over Antarctica and its connections with the Southern America (ATMANTAR)", under process no. 52.0182/2006-5, Proantar/MCT/CNPq. The authors thank the Secretariat of the Interministerial Commission for the Resources of the Sea (SECIRM). Support for the Rothera MF radar was jointly supported by National Science Foundation grant OPP-0839084 and by the UK Natural Environment Research Council. We also thank the TIMED/SABER team, especially M. G. Mlynczak and J. M. Russell, for providing SABER data and J. Fechine for processing these SABER data. Wavelet software used in the present work was provided by C. Torrence and G. Compo and is available at http://paos.colorado.edu/research/wavelets/.

References

Andrioli, V.F., Clemesha, B.R., Batista, P. P. and Schuch, N. J.: Atmospheric tides and mean winds in the meteor region over Santa Maria (29.78° S; 53.88° W), J. Atmos. Sol-Terr. Phys., 71(17–18), 1864–1876, doi:10.1016/j.jastp.2009.07.005, 2009. 16195

Bageston, J. V., Wrasse, C.M., Gobbi, D. Tahakashi, H., and Souza, P. B.: Observation of Mesospheric Gravity Waves at Estação Antártica Comandante Ferraz (62° S), Antarctica, Ann. Geophys., 27, 2593–2598, doi:10.5194/angeo-27-2593-2009, 2009. 16188, 16189

Bageston, J. V., Wrasse, C. M., Hibbins, R. E, Batista, P. P., Gobbi, D., Takahashi, H., Fritts, D. C., Andrioli, V. F., Fechine, J., and Denardini, C. M.: Case Study of a Mesospheric Wall Event over Ferraz Station, Antarctica (62° S), Ann. Geophys., 29, 209-219, doi:10.5194/angeo-29-209-2011, 2011. 16189, 16190, 16194

Chimonas, G. and Hines, C.O.: Doppler Ducting of Atmospheric Gravity-Waves, J. Geophys. Res., 91, 1219–1230, 1986. 16192

ACPD

11, 16185–16206, 2011

Dewan, E. and Picard, R.: Mesospheric bores, J. Geophys. Res., 103, 6295–6305, 1998. 16188, 16193
Dewan, E. and Picard, R.: On the origin of mesospheric bores, J. Geophys. Res., 106, 2921–2927, 2001. 16193
Fechine, J., Medeiros, A. F., Buriti, R. A., Takahashi, H., and Gobbi, D.: Mesospheric bore events in the equatorial middle atmosphere, J. Atmos. Sol-Terr. Phys., 67, 1774–1778, doi:10.1016/j.jastp.2005.04.006, 2005. 16187, 16188
Fechine, J., Wrasse, C. M., Takahashi, H., Medeiros, A. F., Batista, P. P., Clemesha, B. R., Lima, L. M., Fritts, D., Laughman, B., Taylor, M. J., Pautet, P. D., Mlynczak, M. G., and Russell III, J. M.: First observation of an undular mesospheric bore in a Doppler duct, Ann. Geophys., 27, 1399-1406, doi:10.5194/angeo-27-1399-2009, 2009. 16188, 16194
Fritts, D. C. and Yuan, L.: An Analysis of Gravity Wave Ducting in the Atmosphere: Eckart's Resonances in Thermal and Doppler Ducts, J. Geophys. Res., 94(D15), 8,455–18,466, 1989.
Fritts, D. C, Janches, D., Iimura, K., Hocking, W. K., and Bageston, J. V.: Comparisons of mean winds, tides, and gravity wave momentum fluxes measured by enhanced meteor radars on Tierra del Fuego (53.8° S) and King George Island (62° S), J. Geophys. Res., to be submitted, Personal Communication, April 2011. 16192, 16197
Garcia, F. J. and Taylor, M. J.: Two-dimensional spectra-analysis of mesospheric airglow data, Appl. Opt., 36, 29, 7374–7385, 1997. 16191
Hibbins, R. E., Espy, P. J., Jarvis, M. J., Riggin, D. M., and Fritts, D. C.: A climatology of tides and gravity wave variance in the MLT above Rothera, Antarctica obtained by MF radar, J. Atmos. Sol-Terr. Phys., 69, 578–588, doi:10.1016/j.jastp.2006.10.009, 2007. 16189
Isler, J. R., Taylor, M. J., and Fritts, D. C.: Observational Evidence of Wave Ducting and Evanescence in the Mesosphere, J. Geophys. Res., 102, 26301-26313, 1997. 16190
Jarvis, M. J., Jones, G. O. L., and Jenkins, B.: New initiatives in observing the Antarctic mesosphere, Adv. Space Res., 24 (5), 611–619, 1999. 16188, 16192
Laughman, B., Fritts, D. C., and Werne, J.: Numerical simulation of bore generation and morphology in thermal and Doppler ducts, Ann. Geophys., SpreadFEx special issue, 27, 511–523, 2009. 16190
Laughman, B., Fritts, D. C., and Werne, J.: Comparisons of predicted bore evolutions by the Benjamin-Davis-Ono and Navier-Stokes equations for idealized mesopause thermal ducts, J. Geophys. Res., 116, D02120, doi:1029/2010JD014409, 2011. 16188, 16194, 16197
16188, 16194

ACPD
11, 16185–16206, 2011

Manson, A. H., Meek, C. E., Hall, C. M., Nozawa, S., Mitchell, N. J., Pancheva, D., Singer, W., and Hoffmann, P.: Mesopause dynamics from the Scandinavian triangle of radars within the PSMOS-DATAR Project, Ann. Geophys., 22, 367–386, 2004, http://www.ann-geophys.net/22/367/2004/. 16190

Marsh, D. R., Smith, A. K., Mlynczak, M. G., and Russell III, J. M.: SABER observations of the OH Meinel airglow variability near the mesopause, J. Geophys. Res., 111, A10S05, doi:10.1029/2005JA011451, 2006. 16193

Medeiros, A. F., Taylor, M. J., Takahashi, H., Batista, P. P., and Gobbi, D.: An Investigation of gravity wave activity in the low-latitude upper mesosphere: propagation direction and wind filtering, J. Geophys. Res., 108(D14), 4411, 8 pp., doi:10.1029/2002JD002593, 2003. 16189

Medeiros, A., Fechine, J., Buriti, R. A., H. Takahashi, Wrasse, C. M., and Gobbi, D.: Response of OH, O_2 and OI5577 airglow emissions to the mesospheric bore in the equatorial region of Brazil, Adv. Space Res., 35, 1971–1975, doi:10.1016/j.asr.2005.03.075, 2005. 16187

Mertens, C. J., Schmidlin, F. J., Goldberg, R. A., Remsberg, E. E., Pesnell, W. D., Russell III, J. M., Mlynczak, M. G., Lpez-Puertas, M., Wintersteiner, P. P., Picard, R. H., Winick, J. R., and Gordley, L. L.: SABER observations of mesospheric temperatures and comparisons with falling sphere measurements taken during the 2002 Summer MaCWAVE campaign, Geophys. Res. Lett., 31, L03105, doi:10.1029/2003GL018605, 2004. 16191

Narayanan, V. L., Gurubaran, S., Emperumal, K.: A case study of a mesospheric bore event observed with an all-sky airglow imager at Tirunelveli (8.7° N), J. Geophys. Res., 114(D6), D08114, doi:10.1029/2008JD010602, 2009. 16194

Nielsen, K., Taylor, M. J., Stockwell, R., and Jarvis, M.: An unusual mesospheric bore event observed at hight latitudes over Antarctica, Geophys. Res. Lett., 33, L07803, doi:10.1029/2005GL025649, 2006. 16187, 16190, 16192, 16194

Portnyagin, Y. I., Solovjova, T. V., Makarov, N. A., Merzlyakov, E. G., Manson, A. H., Meek, C. E., Hocking, W., Mitchell, N. J., Pancheva, D., Hoffmann, P., Singer, W., Murayama, Y., Igarashi, K., Forbes, J. M., Palo, S., Hall, C., and Nozawa, S.: Monthly mean climatology of the prevailing winds and tides in the Arctic mesosphere/lower thermosphere, Ann. Geophys., 22, 3395–3410, 2004, http://www.ann-geophys.net/22/3395/2004/. 16190

Russell III, J. M., Mlynczak, M. G., Gordley, L. L., Tansock, J., and Esplin, R.: An overview of the SABER experiment and preliminary calibration results, Proceedings of the SPIE, 44th Annual Meeting, Denver, Colorado, 18–23 July, 3756, 277–288, 1999. 16191

ACPD
11, 16185–16206, 2011

She, C. Y., Li, T., Williams, B. P., Yuan, T., and Picard, R. H.: Concurrent OH imager and sodium temperature/wind lidar observation of a mesopause region undular bore event over Fort Collins/Platteville, Colorado, J. Geophys. Res., 109, 22107–22115, doi:10.1029/2004JD004742, 2004. 16194

Smith, S. M., Taylor, M. J., Swenson, G. R., She, C., Hocking, W., Baumgardner, J., and Mendillo, M. A.: Multidiagnostic investigation of the mesospheric bore phenomenon, J. Geophys. Res., 108(A2), 13–18, doi:10.1029/2002JA009500, 2003. 16187, 16193

Smith, S. M., Friedman, J., Raizada, S., Tepley, C., Baumgardner, J., and Mendillo, M.: Evidence of mesospheric bore formation from a breaking gravity wave event: Simultaneuous imaging and lidar measurements, J. Atmos. Sol-Terr. Phys., 67, 345–356, doi:10.1016/j.jastp.2004.11.008, 2005. 16194

Stockwell, R., Taylor, M. J., Nielsen, K., and Jarvis, M. A.: A novel joint space-wavenumber analysis of an unusual Antarctic gravity wave event, Geophys. Res. Lett., 33, L08805, doi:10.1029/2005GL025660, 2006. 16187

Taylor, M.J., Turnbull, D. N. and Lowe, R. P.: Spectrometric and imaging measurements of a spectacular gravity wave event observed during the ALOHA-93 campaign, Geophys. Res. Lett., 20, 2849–2852, 1995. 16187, 16190

Torrence, C. and Compo, G. P.: A practical guide to wavelet analysis, Bulletin of the American Meteorological Society, 79(1), 61–78, 1998.

16195

ACPD
11, 16185–16206, 2011

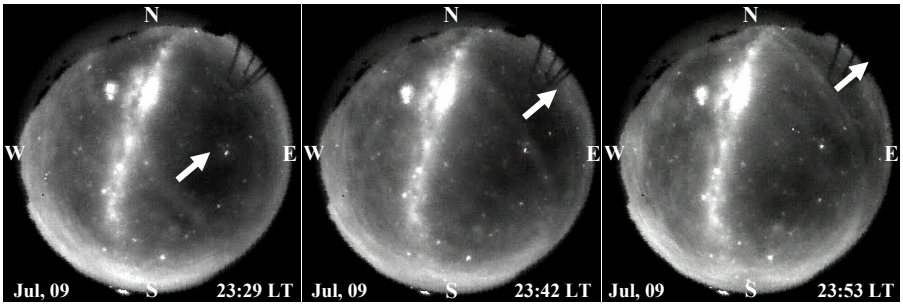

Fig. 1. All-sky OH airglow images at three times spanning 24 min on the night of 9–10 July 2007 showing a mesospheric bore propagating from southwest to northeast.

ACPD
11, 16185–16206, 2011

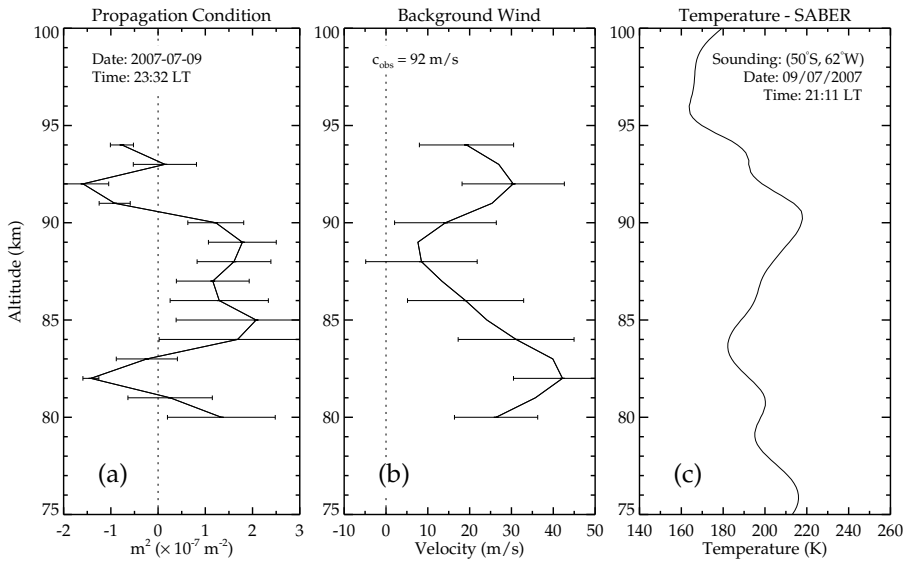

Fig. 2. (a) Vertical wavenumber squared (m^2) showing a duct region between ~84 and ~90 km. **(b)** Wind profile in the bore propagation direction obtained by a MF radar at Rothera Station during the bore observation. **(b)** Temperature profile obtained by SABER on 9 July 2007 to the north of Ferraz and 140 min prior to the bore observation.

ACPD
11, 16185–16206, 2011

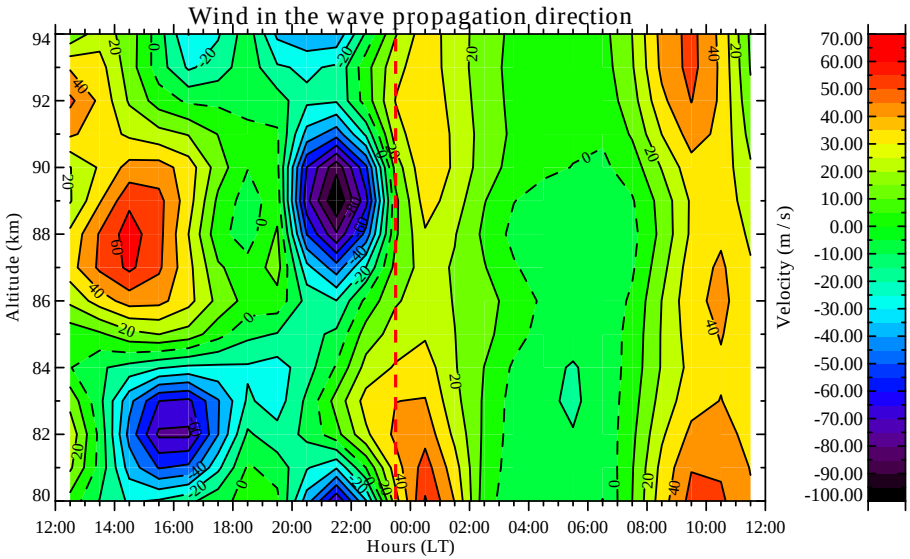

Fig. 3. Contour plot of the Rothera winds in the wave propagation direction, 50° clockwise from north, from 12:00 LT on 9 July to 12:00 LT on 10 July. The vertical dashed red line indicates the time when the wave bore front was at zenith.

ACPD
11, 16185–16206, 2011

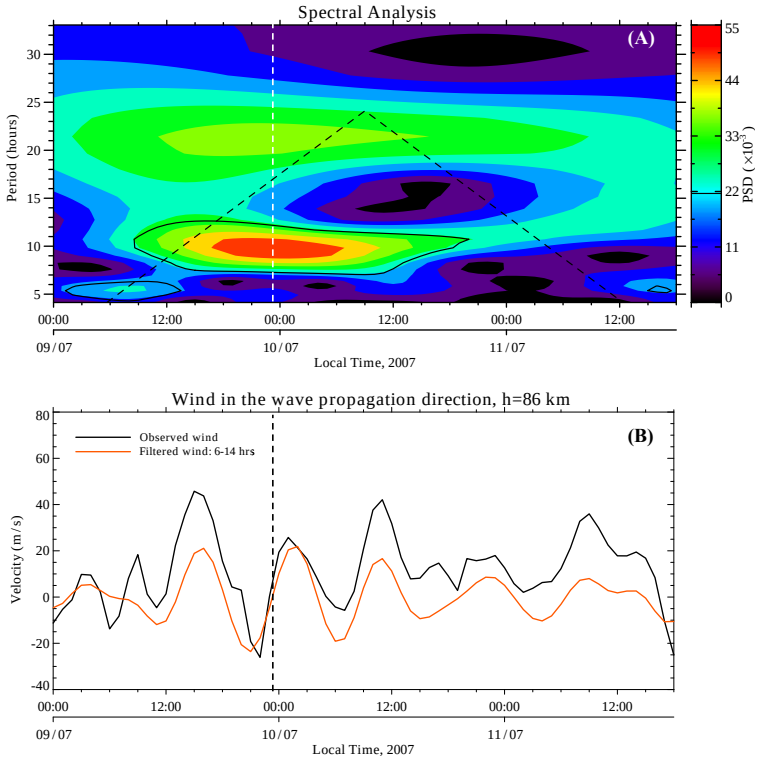

Fig. 4. **(a)** Wavelet spectral analysis of the observed wind at 86 km from 9–11 July showing periods from ~4 to 12 h. Solid black lines indicate confidence levels greater than 90%; dashed black lines show the region uninfluenced by edge effects. **(b)** Wind in the wave propagation direction at 86 km (black line), and a wavelet filtering of the same wind between cutoff periods of 6 and 14 h (red line). Vertical dashed lines indicate the time when the mesospheric bore front was near zenith.

ACPD
11, 16185–16206, 2011

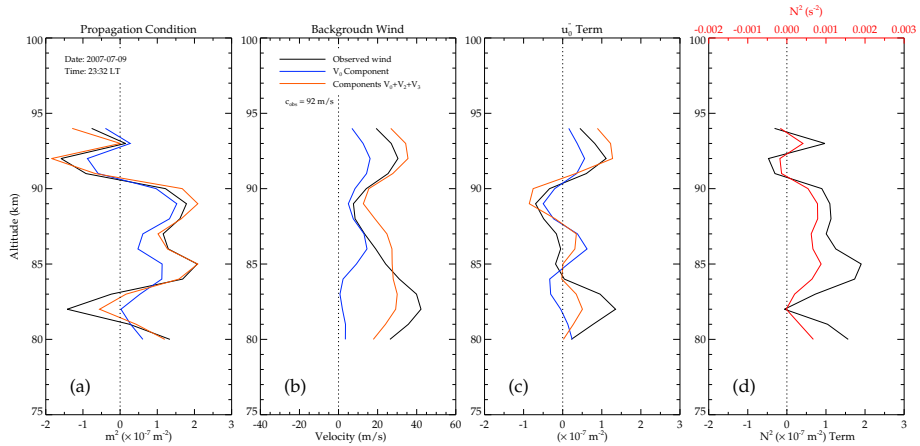

Fig. 5. **(a)** Profiles of m^2 for different wind profiles as shown in **(b)**: observed wind (black); mean wind (without tides, blue) and tidal winds alone (red). **(c)** Curvature terms due to the winds in **(b)**. **(d)** N^2 (red, upper axis) and the buoyancy term contribution to m^2 (black, lower axis) for comparison with panels **(a)** and **(c)**.

ACPD
11, 16185–16206, 2011